

# A 20-40 MHz Ultrasound Transducer for Intravascular Harmonic Imaging

H. J. Vos<sup>1,2</sup>, M. E. Frijlink<sup>1</sup>, E. Droog<sup>1,2,3</sup>, D. E. Goertz<sup>1,4</sup>, G. Blacquièrè<sup>3</sup>, A. Gisolf<sup>2</sup>, N. De Jong<sup>1,4,5</sup>,  
A. F. W. Van der Steen<sup>1,4</sup>

<sup>1</sup>Biomedical Engineering, Erasmus Medical Center, Rotterdam. <sup>2</sup>Delft University of Technology. <sup>3</sup>TNO-TPD Delft.

<sup>4</sup>Interuniversity Cardiology Institute of the Netherlands. <sup>5</sup>University of Twente.

Correspondence: Exp. Echo, room Ee 2302, PO Box 1738, 3000 DR Rotterdam, the Netherlands.

Corresponding e-mail: A.VanderSteen@ErasmusMC.nl

**Abstract**—Recent studies have suggested the feasibility of tissue harmonic imaging (THI) with intravascular ultrasound (IVUS). This paper describes the design, fabrication and characterization of a piezo-electric transducer optimized for tissue harmonic IVUS. Ideally, such a transducer should efficiently transmit a short acoustic pulse at the fundamental transmission frequency and should be sensitive to its second harmonic echo, for which we have chosen 20 MHz and 40 MHz, respectively. The intravascular application limits the transducer dimensions to 0.75 mm by 1 mm. The transducer comprises of a single piezo-electric layer design with additional passive layers for tuning and efficiency improvement, and the Krimholtz-Leedom-Matthaei (KLM) model was used to find iteratively optimal material properties of the different layers. Based on the optimized design a prototype of the transducer was built. The transducer was characterized by water-tank hydrophone measurements and pulse-echo measurements. These measurements showed the transducer to have two frequency bands around 20 MHz and 40 MHz with -6dB fractional bandwidths of 30 % and 25 %, and round-trip insertion losses of -19 dB and -34 dB, respectively.

## I. INTRODUCTION

In the clinical investigation of atherosclerosis, or inflammation of the arteries, intravascular ultrasound (IVUS) catheters are used for imaging a cross section of the artery wall. They form images with either fast-rotating single element transducers or with array configurations. Current IVUS catheters operate in linear imaging mode and as a result they may suffer from limitations such as ring-down, side-lobes in the ultrasound beam and internal reflections of the protecting catheter sheath, which reduce the image quality. From conventional cardiovascular imaging it is known that many of these effects may be reduced with tissue harmonic imaging (THI), in which nonlinear propagation distorts the fundamental frequency pressure pulse, thereby generating higher harmonics [1]. Less harmonic energy is present close to the transducer where the artifacts occur mostly [2]. This beneficial effect comes at the cost of lower signal levels of the harmonics, which can be overcome by careful design of the transducer for harmonic imaging [3, 4].

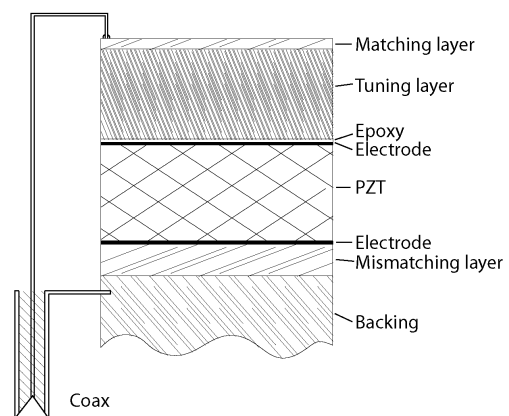


Figure 1. Schematic drawing of the transducer. All passive layers are electrically conducting for easy connection. The transducer aperture is oval sized with axes of 0.75 mm and 1.0 mm.

Initial studies have suggested the feasibility of THI in IVUS imaging [5, 6], but these were carried out with transducers that were not optimized for the purpose. Various harmonic imaging transducers for diagnostic medical high-frequency ultrasound are described in literature [2, 7-9], mostly based on PVDF and lithium niobate. However, compared to PZT ceramics, these materials have a low dielectric constant, which results in a bad electric match to the 50 Ohm electronic circuits if the element size is small. Reported IVUS transducers [10-12] are not optimized for harmonic imaging.

Therefore, a new PZT transducer is developed with dual frequency band sensitivity around 20 MHz and 40 MHz, for mounting on a rotating catheter tip.

## II. METHODS AND FABRICATION

### A. Design

The purpose of the transducer imposes several design constraints. The center frequency of the transmission pulse was chosen to be 20 MHz, resulting in a second harmonic pulse with a center frequency of 40 MHz. These frequencies are thought to give a good trade-off between axial resolution

(which increases with frequency) and penetration depth (which reduces with frequency due to increased acoustic attenuation). As the transducer is mounted inside a catheter tip with 1.3 mm outer diameter (4 French), the aperture should not exceed 0.75 mm by 1.0 mm. The matching layers should be electrically conductive to facilitate connection of the piezo electrodes.

Based on these constraints, a design was made consisting of a single disc of piezo-electric material and two passive layers for frequency tuning and improved acoustic impedance matching (fig. 1). An additional layer is sandwiched between the sound-absorbing backing material and the piezo-electric layer and acts as a so-called mismatching layer [13], increasing the power transmission efficiency in the forward direction.

The transducer was modeled with the one-dimensional Krimholtz-Leedom-Matthaei (KLM) model, which was extended with acoustic and electric energy loss [10, 14-16]. In order to optimize the transducer for harmonic imaging, a multidimensional nonlinear minimization algorithm (Nelder-Mead simplex method) was implemented. Basically, this minimization algorithm searches for the thickness of the active layer and the thickness and acoustical impedances of the passive layers that maximize the transmission efficiency and the reception sensitivity.

This search was associated with the cost function

$$\chi = -\log\{T_f^2(f_0)\} - \log\{T_f^{-1}(2f_0)\}, \quad (1)$$

with  $T_f$  the ratio of the output acoustic force and the source voltage,  $T_f^{-1}$  its reception inverse and  $f_0$  the fundamental frequency (20 MHz). We assumed that the maximum allowed transmission voltage is limited by health care regulations, and due to the squared dependency of the harmonic pressure generation on the fundamental pressure, the cost function relies on the squared transmission function. Logarithms were used for faster convergence.

Values of the piezo-electric material employed in the model corresponded to the material properties of fine-grain high-pressed PZT PPK22 (Stelco GmbH, Neumarkt, Germany), which was chosen for its low loss at high frequencies (mechanic loss factor of 0.02 and electric loss factor of 0.03 at 20 MHz), an electromechanical thickness coupling factor of approximately 0.42 and a relative dielectric constant of approximately 850, measured in accordance with IEEE standards [17].

TABLE I. Optimal Design Values of Material Properties

Layer	Thickness ( $\mu\text{m}$ )	Velocity (m/s)	Z (MRayl)	Loss factor (-)
Matching layer	11	1500 *	4	0.05 *
Tuning layer	64	6400 *	27	0.01 *
Piezo-electric layer	71	5000 *	40 *	0.02 *
Mis-matching layer	14	1500 *	4 *	0.05 *

Based on the available electrically conductive materials (see below), the backing acoustic impedance was set to 7 MRayl and the acoustic impedance of the mismatching layer to 4 MRayl.

The optimized layer properties are given in Table 1. The optimal transducer surface is 1.1 mm<sup>2</sup>, but the size restrictions of the element resulted in an effective area of 0.6 mm<sup>2</sup> (oval aperture with 0.75 mm and 1.0 mm axes). From simulations it followed that this aperture reduction increases the round trip insertion loss by less than 2 dB. The depicted sound velocities and loss factors are measured values of the available materials, on which the prototype is based (see below). Asterixed numbers were manually inserted in the model and kept fixed during the optimization.

### B. Transducer fabrication

A 0.5 mm thick disk of PZT was manually lapped and polished to the appropriate thickness and electroded with a 100 nm nickel film. The tuning layer was made from an aluminum foil (measured impedance of 17 MRayl), rolled to the appropriate thickness and bonded with two-component epoxy under high pressure on the front side of the PZT layer. This epoxy layer was approximately 0.5  $\mu\text{m}$  thick, which is sufficient to maintain electric conductivity due to the surface roughness of the PZT. The second layer and the mismatching layer consisted of 45 / 55 mass percentage mixed silver- and carbon-filled conductive ink (SS477 RFU and SS427, Acheson Industries, Erstein, France) and had a measured acoustic impedance of about 5 MRayl. The backing consisted of silver-filled electrically conductive 2-component epoxy (EccoBond 66C, Emerson and Cuming, Wersterlo, Belgium), which has an acoustic impedance of about 7 MRayl.

Multiple prototype elements were laser-cut into ovals with axes of 1.0 mm and 0.75 mm and mounted on a catheter tip. For the characterization experiments, this tip was attached to a steel tube with 0.9 mm outer diameter. Both sides of the transducer were connected to the coaxial cable (Pico-coax PCX 44 K 11, Grandwill Axon, China) and the element was poled with an electric field of 25 kV/cm at room temperature. The finished transducer is shown in Fig. 2.

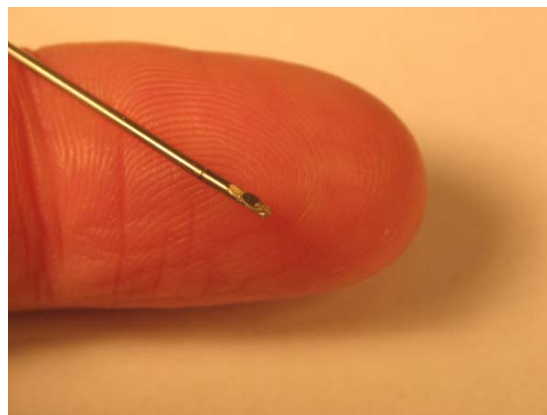


Figure 2. Photograph of the transducer, mounted on a steel tube.

### C. Characterization

The electric impedance of the transducer in air was measured with a vector impedance analyzer (HP 4193A, Hewlett-Packard, Palo Alto, CA, USA), before the cable was attached.

The pressure transfer function of the transducer was measured using a hydrophone in degassed water. The transducer was driven by a 10 V amplitude signal using an arbitrary waveform generator (AWG 520 Tektronix, Portland, OR, USA) in combination with a linear power amplifier (LPI-10 ENI, Rochester, NY, USA). To improve the signal to noise ratio (SNR) for the frequency range of interest (10 MHz to 50 MHz), three separate 100 % fractional bandwidth, Gaussian-enveloped pulses with center frequencies of 20 MHz, 30 MHz and 40 MHz were applied. A needle-type hydrophone (0.075 mm diameter PVDF, Precision Acoustics, Dorchester, UK) was placed on-axis at 4.0 mm distance from the transducer, which is the theoretical natural focal distance at 40 MHz. The received signal was sampled by an 8-bit digitizer (DP235, Acqiris, Geneva, Switzerland) at 400 MHz and averaged over 400 pulses. The pressure transmission transfer function was calculated by the ratio of the hydrophone received spectrum and the amplifier signal spectrum and was compensated for the calibrated hydrophone sensitivity characteristics.

For efficiency measurements in a pulse-echo configuration, the signals were redirected with a passive diode expander/limiter with a measured round-trip signal loss of 12 dB, which was compensated for in the results. A flat stainless steel reflector was placed at 3.3 mm distance parallel to the transducer surface. The transmission pulses were similar to those in the hydrophone measurements and had a 5 V peak amplitude. The received pulse was averaged over 1000 repetitions. The round-trip insertion loss was calculated by the ratio of the received signal spectrum and the AWG transmitted signal spectrum.

The acoustic loss in water at 20 °C is  $2.2 \cdot 10^{-3}$  dB/MHz<sup>2</sup>/cm [18], for which is compensated in the graphs.

### III. RESULTS

Fig. 3 shows the measured electric impedance of the element in air. The passive electric loss resistance was 16 Ohm, estimated from the plot of the real impedance of the transducer in air (not shown here), which was mainly caused by the relatively low electrical conductivity of the mixed silver and carbon layers (about 5 Ohm per layer). The phase plot shows a peak at 22 MHz and 40 MHz. The fact that the lower-frequency peak is not exactly at 20 MHz is attributed to uncertainties associated with the modeling of the epoxy layer between the PZT and the aluminum layer.

Fig. 4 shows the measured transfer function of the transducer at 4.0 mm. It is a graph composed from the three different pulses as described before, plotted in bins with ranges of 10-25 MHz, 25-35 MHz and 35-50 MHz. The transmission transfer function again shows peaks at 22 MHz and at 40 MHz, with -6 dB fractional bandwidths (FBW) of 30 % and 25 %, respectively. Fig. 5 shows the measured

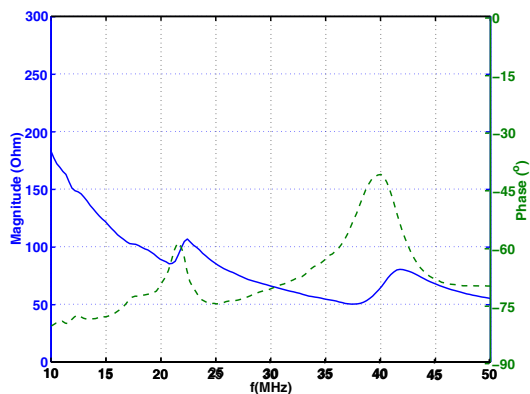


Figure 3. Magnitude (solid) and phase (dashed) of the measured electric impedance of the transducer in air.

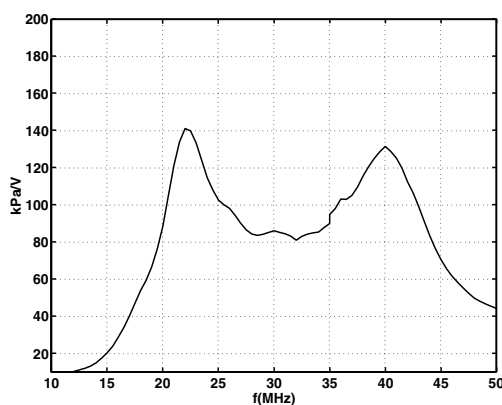


Figure 4. Transfer function of the transducer at 4.0 mm distance in water.

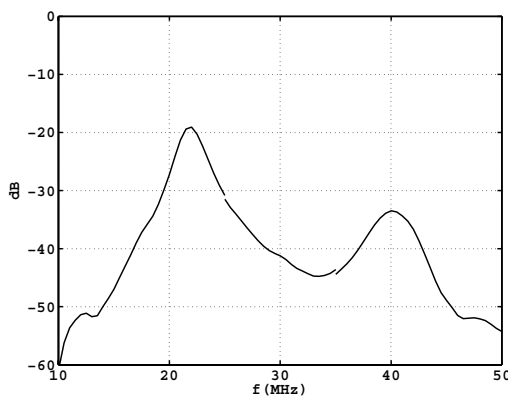


Figure 5. Round-trip insertion loss of the element, measured with a flat steel reflector at 3.3 mm distance.

round-trip insertion loss of the transducer, which shows a value of -19 dB around 22 MHz and -34 dB around 40 MHz.

An ultrasound transducer optimized for harmonic IVUS has been designed, built and characterized.

The modeled optimized properties of the transducer layers were found by the KLM model combined with a nonlinear minimization algorithm. The prototype showed a  $-6$  dB fractional bandwidth around 20 MHz of 30 %, which should be sufficient for a short pulse. The most efficient transmit frequency of the current prototype appeared to be 22 MHz instead of 20 MHz. This frequency could be tuned in future transducers to 20 MHz by adjusting the thickness of the aluminum layer in the design.

The mismatching and the matching layers are the main causes of energy loss, reducing the efficiency and increasing the risk of transducer overheating in a catheter set-up. Using a backing material with lower acoustic impedance, which would eliminate the need for a mismatching layer, could alleviate this problem. This material could also be used for the front matching layer.

The surface area of the prototype is smaller than the most optimal surface area, resulting in an electric mismatch between the transducer and the electrical equipment. However, additional simulations showed that this gave a round trip insertion loss increase of less than 2 dB, which is negligible compared to the losses described above.

Further research will focus on better understanding of the influence of the epoxy adhesive layer, and on a comparison of the transducer with the KLM-model in the water-tank experiments.

## ACKNOWLEDGMENTS

We would like to thank Gerrit van Dijk for his major contribution to the fabrication of the transducer. The Dutch Technology Foundation STW financially supports this work (Project RPG5442).

- [1] F. A. Duck, "Nonlinear acoustics in diagnostic ultrasound", *Ultrasound in Medicine and biology*, vol. 28, pp. 1-18, no. 1, 2002
- [2] E. W. Cherin, J. K. Poulsen, A. F. W. v. d. Steen, P. Lum and F. S. Foster, "Experimental characterization of fundamental and second harmonic beams for a high-frequency ultrasound transducer", *Ultrasound in Medicine and biology*, vol. 28, pp. 635-646, no. 5, 2002
- [3] S. Saitoh, M. Izumi and Y. Mine, "A Dual Frequency Ultrasonic Probe for Medical Applications", *IEEE transact. on Ultrasonics, Ferroelectrics, and Frequency Control*, vol. 42, pp. 294-300, no. 2, 1995
- [4] S. Takeuchi, M. R. A. A. Zaabi, T. Sato and N. Kawashima, "Ultrasound Transducer with Double-Peak Frequency Characteristics for Subharmonic Imaging", *Japanese Journal of Applied Physics*, vol. 42, pp. 3253-3254, no. 1 - 5B, 2003
- [5] A. F. W. v. d. Steen, J. K. Poulsen, E. Cherin and F. S. Foster, "Harmonic imaging at high frequencies for IVUS", *IEEE Ultrasonics Symposium*, pp. 1537-1540, 1999
- [6] M. E. Frijlink, D. E. Goertz, F. S. Foster and A. F. W. v. d. Steen, "High Frequency Harmonic Imaging In Presence of Intravascular Stents", *IEEE Ultrasonics Symposium*, pp. 208-211, 2003
- [7] A. Fleischmann, R. Modi, A. Nair, J. Talman, G. Lockwood and S. Roy, "Miniature high frequency focused ultrasonic transducers for minimally invasive imaging procedures", *Sensors and Actuators A*, vol. 103, pp. 76-82, no. 2003
- [8] Q. F. Zhou, J. Cannata, C. Z. Huang, H. K. Guo, V. Marmarelis and K. K. Shung, "Fabrication and Modeling of Inversion Layer Ultrasonic Transducers Using LiNbO<sub>3</sub> Single Crystal", *IEEE Ultrasonics Symposium*, pp. 1034-1037, 2003
- [9] R. J. Meyer, S. Alkoy, R. Newnham and J. Cochran, "Development of Materials and Composites for >25 MHz Single Element Transducers", *IEEE Ultrasonics Symposium*, pp. 1299-1302, 1999
- [10] F. S. Foster, L. K. Ryan and D. H. Turnbull, "Characterization of Lead Zirconate Titanate Ceramics for Use in Miniature High-frequency (20-80MHz) Transducers", *IEEE transact. on Ultrasonics, Ferroelectrics, and Frequency Control*, vol. 38, pp. 446-453, no. 5, 1991
- [11] O. Oralkan, A. S. Ergun, J. A. Johnson, M. Karaman, U. Demirci, K. Kaviani, T. H. Lee and B. T. Khuri-Yakub, "Capacitive Micromachined Ultrasonic Transducers: Next generation arrays for acoustic imaging?" *IEEE transact. on Ultrasonics, Ferroelectrics, and Frequency Control*, vol. 49, pp. 1596-1610, no. 11, 2002
- [12] J. G. Knight and F. L. Degertekin, "Fabrication and Characterization of cMUTs for Forward Looking Intravascular Ultrasound Imaging", *IEEE Ultrasonics Symposium*, pp. 577-580, 2003
- [13] J. Souquet, P. Defranould and J. Desbois, "Design of low-loss wide-band ultrasonic transducers for noninvasive medical applications", *IEEE transact. on Sonics and Ultrasonics*, vol. SU-26, pp. 75-81, no. 2, 1979
- [14] M. Lethiecq, L. P. Tran-Huu-Hue, F. Patat and L. Pourcelot, "Measurement of Losses in Five Piezoelectric Ceramics Between 2 and 50 MHz", *IEEE transact. on Ultrasonics, Ferroelectrics, and Frequency Control*, vol. 40, pp. 232-237, no. 3, 1993
- [15] G. S. Kino, *Acoustic Waves: Devices, imaging and analog signal processing*, Prentice-Hall Inc., 1987, pp. 154-163
- [16] R. Krimholtz, D. A. Leedom and G. L. Matthaei, "New equivalent circuits for elementary piezoelectric transducers", *Electronic letters*, vol. 6, pp. 389-399, no. 13, 1970
- [17] ANSI/IEEE 176 standard on Piezoelectricity, 1987
- [18] F. A. Duck, *Physical properties of tissue*, Academic press Ltd., 1990, p. 95